A novel Composite Smeared Finite Element for Mechanics (CSFEM) – some applications

Vladimir Simic[a,b], Miljan Milosevic[a,b,c], Vladimir Milicevic[c], Nenad Filipovic [b,e], Milos Kojic[b,d,f,*]

[a]Institute for Information Technologies, University of Kragujevac, Department of Technical- Technological Sciences, Jovana Cvijica bb, 34000 Kragujevac, Serbia

[b]Bioengineering Research and Development Center BioIRC Kragujevac, Prvoslava Stojanovica 6, 34000 Kragujevac, Serbia.

[c]Belgrade Metropolitan University, Tadeusa Koscuska 63, 11000 Belgrade, Serbia.

[d]Houston Methodist Research Institute, The Department of Nanomedicine, 6670 Bertner Ave., R7 117, Houston, TX 77030, USA

[e]University of Kragujevac, Faculty for Engineering Sciences, Sestre Janic 6, 34000 Kragujevac, Serbia.

[f]Serbian Academy of Sciences and Arts, Knez Mihailova 35, 11000 Belgrade, Serbia. *Corresponding author: mkojic42@gmail.com (M.Kojic), Houston Methodist Research Institute, The Department of Nanomedicine, 6670 Bertner Ave., R7 117, Houston, TX 77030.

Abstract

Background: Mechanical forces at the micro-scale level have been recognized as an important factor determining various biological functions. The study of cell or tissue mechanics is critical to understanding problems in physiology and disease development. **Objective:** The complexity of computational models and efforts made for their development in the past required significant robustness and different approaches in the modeling process. **Method:** For the purpose of modeling process simplifications, smeared mechanics concept was introduced by M. Kojic as a general concept for modeling the deformation of composite continua. A composite smeared finite element for mechanics (CSFEM) was formulated which consists of the supporting medium and immersed subdomains of deformable continua with mutual interactions. Interaction is modeled using 1D contact elements (for both tangential and normal directions), where the interaction takes into account appropriate material parameters, as well as the contact areas. **Results:** In this paper we have presented verification examples with applications of the CSFEMs that include the pancreatic tumor tissue, nano-indentation model and tumor growth model. **Conclusions:** We have described composite smeared finite element for mechanics (CSFEM) and contact elements between compartments that can interact. Accuracy and applicability are determined on two verification and tumor growth example.

Key-words: smeared mechanics, tissue mechanics, composite smeared finite element, tumor growth

INTRODUCTION:

Cells inside the human body represent complex biological constituents (with viscoelastic behavior) that can absorb the physico-chemical and mechanical signals and stimuli from surrounding tissues and have an appropriate and active response by triggering cell growth, proliferation, differentiation, motility, etc. Forces that act on cells and surrounding space, such as shear force, loading force, stress, and strain, control various biological activities and responses to drugs. Smeared modeling concept is previously formulated and introduced in reference [1], with significant modifications presented in reference [2]. On the other hand, the extracellular matrix (ECM) is a complex and dynamic network that surrounds cells in all tissues, providing structural and mechanical support, and mediating diverse biological processes that are crucial for supporting tissue formation and function [3]. ECM serves as a binding (supporting) medium which integrates cells and shapes groups of cells into tissues and organs with defined biological and mechanical functions. There are a large number of studies showing that mechanical interactions between cells and ECM play an important role in biological processes. Tissue models that consist of specified cells and ECM components provide simplified biological systems suitable for studying cell-matrix interactions in tissue development [4, 5]. Also, quantitative measurements of the force exerted by these models provide a powerful and flexible approach to studying mechanisms of force impact on ECM-cells interaction [6, 7]. Measurements of tissue stiffness introduce additional data and the possibility to reveal mechanical functions of matrix components and cellular structural systems such as the cytoskeleton, which offers the possibility to model complex fibrous structures inside extracellular space.

From the listed publications follows the complexity of computational modeling of physical fields and its representation (within a small tissue part in the human body, as well as in a specific organ), therefore it is desirable to have a computational methodology more feasible, more robust, and less-demanding for practical applications. In physics, engineering, or medical science, composite media are mostly present, such as in geology according to [8] or in living organisms [9] (tissue, biological fluids), as well as in fracture mechanics where finite element method is applied [10]. Besides the

existing composite-based models (developed in other science fields), the novel smeared concept is here applied to modeling the mechanical behavior of tissue and different types of cells (cancerous or healthy ones).

A traditional approach to modeling problems within composite media is to divide the entire space into subdomains occupied by a basic constituent, with the corresponding laws and properties, and formulate the subdomain models. The next step is to model the interactions between the basic domain and immersed subdomains at common boundaries and solve for the unknowns describing the problem. This approach requires significant effort to specify all internal boundaries between domains, but this approach is almost not applicable to larger domains of tissue composed of complex extracellular space, cells, cell organelles, etc. This is a motivation to formulate simplified models which take into account media complexity, but still have satisfactory accuracy compared to the effort necessary for modeling complex models.

Our previous research was related to a smeared concept for mass transport in the capillary system and tissue [11-14] with a demonstrated applicability and accuracy concerning traditional modeling methods. The concept is implemented into the in-house code PAK [14]. In this paper we present the applicability and accuracy of the method on a simple test model, and further, we compare real detailed geometry models and smeared representations; finally, the smeared model gives an insight into a tumor growth model. Regarding the tumor growth process, in our paper [16] we have managed to couple a tumor growth model embedded in a microenvironment, with a bio distribution model of a whole organ. This coupling method offered a better insight into regulation of the oxygen diffusion and possibility to include other therapeutic agents' molecules (i. e. chemotherapeutics). Next step was to introduce mechanical behavior of tumor due to prescribed volumetric growth inside cancer cells.

METHODS:

In this section, we first give the basic finite element balance equations and then summarize the formulation of the composite smeared finite element (CSFEM) as the fundamental element for the smeared methodology in mechanics. The steps are analogous to those in [1] and are given in [2].

Equations described below (used for formulating CSFEM) are integrated in the FE software, PAK (abbreviation in Serbian of 'Program za Analizu Konstrukcija' - 'Program for Structural Analysis'). The software was originally developed at the University of Kragujevac, followed by research within BioIRC (Bioengineering Research and Development Center, Kragujevac, Serbia). It represents a high-performance finite element analysis (FEA) software, tested and implemented over several decades [14], for solving general engineering problems and further extended to complex coupled multi-physics/multi-scale problems. Regarding the graphical representation, the CAD Field & Solid is the University of Kragujevac and BioIRC's in-house pre- and post-processing 3D modeling and visualization tool developed over 20 years using the C++ programming language and the MFC (Microsoft Foundation Class) library. The main advantage of using this software is the simplification of the generation model process and ability to visualize, animate and easy- to- analyze the results.

Regarding the pre-processing part, the CAD software is used in a form that can be run by the FE simulation code PAK. The FE model data containing a FE mesh, with accompanied material data, are exported to a file with extension *.dat .. The results of a FE simulation (i.e. field of displacements or other quantities) are exported to a file with extension *.unv, automatically imported by the CAD postprocessor. The CAD post-processor tool is used for importing and visualization of the computed results, and analysis by plotting various representations (as, for example, tumor radius versus time). Various options in the CAD offer to users inspection of the results or parametric studies.

Composite smeared finite element for mechanics (CSFEM)

The basic goal of the smeared model is to formulate a composite continuum finite element (CSFEM) that will take into account constituents of the true physical fields (continuum and 1D domains) that correspond to the "detailed" model (Fig 1.a). It is assumed that each of the compartments (showed in Fig. 1a as separate domains with their boundaries) has its own FE mesh of continuum elements, while for 1D domains we use 1D finite elements for modeling media such as blood vessels, fibers, cytoskeleton, etc. Considering the complexity of the presented detailed model, which requires significant effort for the model preparation and generation, in this case, it would be an impractical or even impossible task to achieve. Simplification of this model is shown in Fig. 1.b, where the smeared

model is presented with a corresponding supporting domain that represents extracellular space (ie. the basic medium notated with the index *b*), and two immersed domains with noted velocities at contact boundaries (Cell 7 and Cell 8, Fig. 1c and d). The main goal is a formulation of the equivalent computational model, less demanding to achieve its geometry, with satisfactory accuracy concerning detailed representation. Presentation of the methodology is according to the basic concept given in [1], with significant modifications in the reference [2].

[Place Figure 1 here]

General expressions for the virtual power for composite media

As can be seen from Figure 1d, there is a presence of a supporting medium (or the basic medium, with the index '*b*' Fig 1.d) in which are immersed other deformable bodies or domains (compartments).

Let's denote the velocity field within a domain '*k*' as vectors $\mathbf{v}^k$. At the contact boundary between any immersed domain and the supporting medium, velocities for the supporting medium *b* and the domain *k* are expressed in the local coordinate system,

$$\mathbf{v}^b = v_n^b \mathbf{n}^k + v_t^b \mathbf{t}^k, \qquad \mathbf{v}^k = v_n^k \mathbf{n}^k + v_t^k \mathbf{t}^k \tag{3}$$

where v_n^b, v_n^k and v_t^b, v_t^k are the velocity components in the direction of the boundary normal $\mathbf{n}^k$ and tangent $\mathbf{t}^k$. The relative velocities at the boundaries are

$$v_i^{nrk} = v_i^{nk} - v_i^{nb}, \quad v_i^{trk} = v_i^{tk} - v_i^{tb} \tag{4}$$

where v_i^{nrk} and v_i^{trk} are relative velocities at the boundaries in normal and tangential direction, respectively. At the boundary between two domains '*k*' and '*k*+1' we have the relative velocities (*r*) in normal (*n*) and tangential direction (*t*)

$$v_i^{nrk,k+1} = v_i^{nk+1} - v_i^{nk}, \quad v_i^{trk,k+1} = v_i^{tk+1} - v_i^{tk} \tag{5}$$

Normal stresses, that are present at the interaction surface, are denoted as σ^{nk} while component of stress due to sliding between a compartment *'k'* and the supporting medium is $\boldsymbol{\tau}^{bk}$, and between '*k*' and '*k*+1' is $\boldsymbol{\tau}^{k,k+1}$.

Elementary surfaces, between the supporting medium *b* and the medium '*k*', and between two media *k* and *k+1* are dA^{bk} and $dA^{k,k+1}$, respectively; and the projections of these surfaces on the coordinate directions are dA_i^{bk} and $dA_i^{k,k+1}$.

Finally, the expression for virtual power due to both normal and tangent stresses is

$$\delta W^{stress} = \sigma_{ij}^{b}\delta\dot{e}_{ij}^{b}dV^{b} + \sum_{k=1}^{N_d}\sigma_{ij}^{k}\delta\dot{e}_{ij}^{k}dV^{k} + \sum_{k=1}^{N_d}\tau^{bk}\delta v_t^{rbk}dA^{bk} + \sum_{k=1}^{N_d-1}\tau^{k,k+1}\delta v_t^{k,k+1}dA^{k,k+1} \tag{6}$$

where $\delta\dot{e}_{ij}^{b}$, $\delta\dot{e}_{ij}^{k}$ and $\dot{e}_{ij}^{b}$, $\dot{e}_{ij}^{k}$ are the strain rate variations and the strain rates within supporting medium and domain *k*, respectively. The virtual power due to inertial forces is

$$\delta W^{in} = -\rho^{b}\dot{v}_i^{b}\delta v_i^{b}dV^{b} - \sum_{k=1}^{N_d}\rho^{k}\dot{v}_i^{k}\delta v_i^{k}dV^{k} \tag{7}$$

where ρ^{b} and ρ^{k} are densities of the supporting and corresponding '*k*' domain, respectively.

Finite element balance equations

The above expressions serve as the basis for the formulation of the FE balance equations. The solids of interest are discretized into finite elements. Finite element balance equations for continuum space, for a time step Δt and iteration *i*, have a standard form [9],

$$\left(\frac{1}{\Delta t}\mathbf{M} + \mathbf{K}^{(i-1)}\right)\Delta\mathbf{V}^{(i)} = \mathbf{F}^{ext} - \mathbf{F}^{\mathrm{int}(i-1)} + \mathbf{F}^{in(i-1)} \tag{8}$$

where $\Delta\mathbf{V}^{(i)}$ are nodal velocity increments for the current iteration *i*, $\mathbf{F}^{ext}$ are external forces at the element nodes; $\mathbf{F}^{\mathrm{int}(i-1)}$ and $\mathbf{F}^{in(i-1)}$ are internal forces due to stresses and inertial forces according to the previous iteration (*i-1*). In general, the matrices and nodal vectors can be expressed as [1]

$$\mathbf{M} = \int_V \rho \mathbf{N}^T \mathbf{N} dV, \quad \mathbf{K} = \int_V \mathbf{B}^T \mathbf{C} \mathbf{B} dV$$
$$\mathbf{F}^{\text{int}(i-1)} = \int_V \mathbf{B}^T \boldsymbol{\sigma}^{(i-1)} dV, \quad \mathbf{F}^{in(i-1)} = -\mathbf{M}\dot{\mathbf{V}}^{(i-1)} \tag{9}$$

where **M** is the element mass matrix, **K** is the stiffness matrix, ρ is the density of the material, **N** is the interpolation matrix, **B** is the geometric matrix with the derivatives to spatial coordinates; **C** is the constitutive matrix, $\boldsymbol{\sigma}^{(i-1)}$ is the stress tensor; $\dot{\mathbf{V}}^{(i-1)}$ is acceleration according to the previous iteration. Other details may be found elsewhere [9].

Formulation of composite smeared finite element applied for mechanics (CSFEM)

Here, we summarize a smeared FE formulation for mechanics presented in [1, 2]. The finite element space is divided into domains that are immersed within the supporting medium as schematically shown in Fig. 2. Volumes of the domains are specified by the volumetric fractions r_v^k with respect to the total element volume *V*,

$$V^k = r_v^k V \tag{10}$$

[Place Figure 2 here]

and the volumetric fraction r_V^b of the supporting medium (*b*) is

$$r_V^b = 1 - \sum_{k=1}^{N_d} r_V^k \tag{11}$$

At a contact surface, between two media, we formulate two contact elements (so-called connectivity elements) one in the normal direction (*n*) and the other in the tangential (*t*) direction. Regarding the contact elements, the nodal normal and tangential forces F_{Ji}^n and F_{Ji}^t at a FE node *J*, in directions of the global axes x_i, are

$$F_{J_i}^n = K_{IJ}^{n(k,k+1)} \left(V^{k+1} - V^k \right)_{Ji}^{(i-1)} \left(r_{Ai}^n \right)_J \tag{12}$$

and

$$F_{Ji}^{t} = -K_{IJ}^{t(k,k+1)} \left(V^{k+1} - V^{k} \right)_{Ji}^{(i-1)} \left(r_{Ai}^{t} \right)_{J} \tag{13}$$

where $\left(r_{Ai}^{n} \right)_{J}$ and $\left(r_{Ai}^{t} \right)_{J}$ are the area fractions of surfaces A^n and A^t, in directions of the global coordinate axes x_i, with respect to the area A^k

$$r_{Ai}^{n} = \frac{A_i^n}{A^k}, \quad r_{Ai}^{t} = \frac{A_i^t}{A^k}, \tag{14}$$

where $A^k = r_{AV}^k V$ is the area of the contact surface and r_{AV}^k is the area-to-volume ratio, or the area ratio; A_i^i and A_i^n are the absolute values of the area projections. In the case of a 2D model we have $r_{Ax}^{t} = r_{Ay}^{n}$, $r_{Ay}^{t} = r_{Ax}^{n}$.

The matrices $K_{IJ}^{n(k,k+1)}$ and $K_{IJ}^{t(k,k+1)}$ for a FE node *J* and directions *i*=1,2,3, are:

$$K_{11}^{n(k,k+1)} = K_{22}^{n(k,k+1)} = -K_{12}^{n(k,k+1)} = -K_{21}^{n(k,k+1)} = \left[\left(k_n r_V r_{AV} r_{A_i}^{n} \right)^{k} + \left(k_n r_V r_{AV} r_{A_i}^{n} \right)^{k+1} \right]_J V$$

$$K_{11}^{t(k,k+1)} = K_{22}^{t(k,k+1)} = -K_{12}^{t(k,k+1)} = -K_{21}^{t(k,k+1)} = 0.5\eta_{k,k+1} \left[\left(r_V r_{AV} r_{A_i}^{t} \right)^{k} + \left(r_V r_{AV} r_{A_i}^{t} \right)^{k+1} \right]_J V \tag{15}$$

where k_n and η are the stiffness and viscous resistance coefficients for the contact surfaces *k* and *k+1*, respectively. Other details, regarding the contact between domains, are given in [2].

RESULTS:

This section is devoted to a presentation of several examples, first for the verification of the smeared mechanics concept- a comparison of the real pancreatic tumor tissue geometry to its smeared representation, and nano indentation example. Finally we present the tumor growth model, at the end of this section.

Verification of the CSFEM on a simple uniaxial tension examples

Verification of the smeared mechanics methodology applicability is performed on a comparison of detailed and smeared models without sliding conditions between all subdomains and supporting medium.

Detailed model of pancreatic tumor tissue and equivalent smeared model.

We here examine a 2D model of pancreatic tumor tissue with a real distribution of cells and extracellular space (exploited from CT image; Fig. 3a). Here we take extension load uniformly distributed at the right boundary, just over the extracellular material. The applied load increases linearly to the maximum force value of 4,000 N at time t=5.0s and decreases back to zero.

[Place Figure 3 here]

The model is rectangular-shaped (48.5 x 38.2 mm), with 80 irregular-shaped cells embedded into the extracellular space, here considered as the supporting medium, with different material properties than applied to cells. The material model used for both domains is linear-elastic (close to incompressible) with the Poisson ratio $\nu = 0.49$. Young's modulus for the extracellular space is $E = 2000$ N/mm^2. The analysis considered a case where Young's moduli are equal (default value $E = 2000$ N/mm^2) in both domains. Material density is taken to be 10^{-3} g/mm^3. Regarding geometry data for the detailed model, the mesh shown in Fig. 3a contains 13,927 FE nodes, while the number of 2D FEs is 12,739.

Compared to the smeared model, we used only 16 2D CSFEM elements (Fig. 3b) and 25 FE nodes, to model two domains – cells and extracellular space. The volumetric fraction for the cell domain is $r_V = 0.517$ (coverage of almost 52% of the entire space), average area fraction coefficient is $r_{AV} = 0.411$, and the tangent area fractions in both coordinate directions are taken to be equal (irregular cells shape approximately corresponds to a circular shape), $r_{AVx} = r_{AVy} = 0.636$. The assumption is that there is no slipping between the cells and the extracellular space domain.

Figure 4 shows the displacement field in the x-direction for the detailed (a) and smeared model (b) for three characteristic time steps (material model and material parameters are the same for both models and their domains). There is a fairly good matching of the results between the two models, when the

tension reaches both the maximum values (Fig. 4; t = 5.0s) and random loading and unloading regimes (Fig. 4; t = 2.5s and 7.5s).

[Place Figure 4 here]

We also have examined the case when Young's modulus of the extracellular space in the supporting medium (E_{supp} = 1000 N/mm^2) is two times smaller than in cells (compartment) domain (E_{cell} = 2000 N/mm^2). Compared to previous case (with the equal Young's moduli in both domains), it can be seen that, under the same force on the supporting medium, displacements of the supporting domain (tissue domain in the detailed model), at the maximum extension, are 25 percent larger (6.51 for the case with equal moduli, 7.82 for different moduli). This is due to the less stiff cell material.

Nano-indentation example

First, we have examined a nano-indentation example with experimental data used from Laboratory in Basel [15]. The indentation-type procedure has evolved during the last decade as an approach used to measure nano-scale stiffness of different types of lesions biopsies (i.e. breast) at the cellular level. An example of individual 20 × 20 μm AFM (Atomic-Force Microscopy) stiffness maps collected across the entire surface of fresh biopsy specimens. is shown on Fig 5a. The model used in our case is shown in Fig. 5b; it is square-shaped (100x50 mm), consisting of a supporting medium and embedded compartment, with different material properties. The material model used for both domains is linear-elastic (close to incompressible) with the Poisson ratio ν = 0.49. Young's modulus for the supporting medium is E = 1000 N/mm^2. Regarding material parameters for compartment Young's moduli are two times smaller than in the supporting domain (E = 500 N/mm^2). Material density is taken to be 10^{-3} g/mm^3, for both domains. Volumetric fraction of cells is r_V = 0.7, average area fraction coefficient is r_{AV} = 0.411, and the tangent area fractions in both coordinate directions are taken to be equal- r_{AVx} = r_{AVy} = 0.636. The resistance coefficient is set to be 10.0. Here, we consider a case without slipping between the supporting domain and compartment. Regarding geometry data, the mesh shown in Fig. 5b contains 5151 FE nodes, while the number of 2D FEs is 5004. The simulation lasts for 20 steps; with duration of one step is 0.5s.

[Place Figure 5 here]

Figure 6 shows the displacement field in the x-direction for the nano-indentation model for one characteristic time step. Indentation force is applied on two nodes on the right boundary of the model and, due to symmetry; results are shown for a mirrored model around the axis of symmetry. It is notable that, comparing supporting domain displacements with and without slipping involved, in case of slipping has a larger value due to the sliding coefficient. Also, regarding compartment deformation, displacements of the compartment have the smallest values concerning the supporting domain due to sliding allowed by a smaller resistance coefficient and smaller value of Young moduli.

[Place Figure 6 here]

Displacements vs applied indentation force diagram are shown in Figure 7. It refers to the linear growth of displacements, especially for supporting domain, accompanied by the growth of indentation force. Followed by the displacement field in Fig 6, it is notable that the highest values are in the case of slipping for the supporting domain, and the lowest increase of displacement is in the case of the compartment, due to the sliding resistance.

[Place Figure 7 here]

Application of the CSFEM to tumor growth

The cancer remains the second (17.8%) diseases of the total deaths per a year, just behind the heart diseases (20.6%). These large numbers, related to cancer, do not change significantly over years in spite of enormous effort, both from clinicians and biomedical engineers. Many approaches and computational models have been introduced, from the agent-based modeling, reviewed in [18], up to a hybrid-type model where the tumor space is divided into regions with descriptions on the cell level, and others as continua [19].

This section is devoted to the application of our smeared model concept to tumor growth modeling concept. The model consists of a circular tumor that can grow due to the increasing volume of cancerous (tumor) cells. The tumor domain is surrounded by tissue of circular shape. Due to

symmetry, only ¼ of the entire space is modeled (Fig. 8a), with the no-displacements through symmetry planes as boundary conditions. The CSFE is used (Fig 8b, CAD representation), with the extracellular space as the supporting medium in the tumor and the surrounding. Two groups of cells are immersed within the supporting medium: healthy cells in the entire domain and tumor cells within the tumor, with their volumetric fractions.

The mass growth in this model is achieved by using the following procedure. The rate of the volumetric deformation due to the tumor growth is given as

$$\frac{d\left(\Delta V^{growth}\right)}{dt\Delta V} = \frac{c_{mass}^{growth}}{\rho_{mass}^{growth}} = \frac{d(\Delta V)}{dt\Delta V} = \dot{e}_V \tag{16}$$

where $c_{mass}^{growth}\left[\frac{kg}{m^3 s}\right]$ is the mass rate constant, ρ_{mass}^{growth} is the density of additional mass and $\dot{e}_V$ is volumetric strain rate. The mass rate constant is taken from the [17].

In the implementation of our FE software [14], we used the volumetric strain rates to be the same in each coordinate direction. In 2D plane strain case, we have

$$\dot{e}_{xx}^{V} = \dot{e}_{yy}^{V} = 0.5\dot{e}_V \tag{17}$$

Stress increment due to a volumetric growth is

$$\left(\Delta\boldsymbol{\sigma}\right)_{jj} = r_V\left(\mathbf{C}\Delta\mathbf{e}^{V}\right)_{ij} \tag{18}$$

where **C** is the constitutive matrix, and r_V is volumetric fraction of cells. This stress increment is added to current stress of the material element, for the current time step.

For the purpose of this paper, we have created parametric type of model, in order to simulate tumor growth process on different types and tumor geometries. Using custom made dialogs (in early mentioned software package CAD), we were able to define model radius, mesh structure, volumetric growth constants and material model used for each of the model domains.

We have used one default radius of tumor- R_{tum}=3 mm and the surrounding tissue radius is constant R_{tiss} =10mm. The material of the healthy cells and extracellular space is linear-elastic, with the Young modulus E = 100 [N/mm^2], and the Poisson coefficient v= 0.49, close to incompressibility condition. The volumetric fraction of tumor cells (within the tumor domain) is in the range r_{Vtum} = 0.3-0.5-0.7,

while the area fraction coefficient r_{AV} = 0.56; and the tangent and normal area fractions in both coordinate directions are equal- r_{AVx} = r_{AVy} = 0.636 (circular cell shape, calculated using (12)). The volumetric fraction of healthy cells is r_{Vcell} = 0.1 and r_{Vcell} = 0.6 within the tumor domain, and outside the tumor, respectively; therefore, the volumetric fraction of the extracellular space is calculated as r_{Vex}=1-r_{Vcel}- r_{Vtum}. Two cases are considered: without and with slipping (sliding) between compartments. It is assumed that tumor growth rate is a constant value, with a volumetric strain rate of 0.25/day, which is 0.25g/(gday). The time of our analysis in all models is 20 days, divided into 10 equal time steps.

[Place Figure 8 here]

Displacements solutions for the case without slipping between compartments, with an initial radius R_{tum}=3mm, are displayed in Fig. 9. It displays tumor growth for three volumetric fractions of tumor cells after 10 and 20 days (in the middle and at the end of the simulation). Note that Young moduli and Poison's ratio are the same as for the other compartments (E = 100 [N/mm^2], v= 0.49). As we have expected, it is obvious that the growth is faster in case of an increased volumetric fraction of tumor cells. The increase of the tumor radius over time is shown in Fig. 10 which displays the numerical aspect of the tumor growth process.

[Place Figure 9 here]

[Place Figure 10 here]

Another case which we have considered is the one with prescribed internal radius- R_{tum} = 7mm, where we analyzed how volumetric fractions inside a specified domain affect growth. Results in Figure 11, for two time steps, show that the overall displacements are larger when compared to the previous case (over 95 percent approximately) which was expected. Figure 12 displays the growth of tumor radius for three selected volumetric fractions.

[Place Figure 11 here]

[Place Figure 12 here]

CONCLUSIONS:

In this paper, we have presented the smeared modeling concept for the mechanical field, with necessary steps and basic equations for formulating this concept according to our previous works-. The composite smeared finite element for mechanics (CSFEM) is described, derived using the virtual power for composite media and contact elements between compartments that can interact. Significant advance is demonstrated by implementation of the methodology into the FE simulation software and presented results. Accuracy and applicability of this methodology are assessed on two verification examples. The first example examined a uniaxial tension of pancreatic tumor tissue where we have demonstrated a fairly good agreement of the results between the smeared and detailed models, including the case when Young's modulus is not equal in all domains. Another example is a nano-indentation problem which shows the potential to model a complex indentation process. Further application to this problem assumes comparison with experiments and use of a large results database. Further generalization of the smeared methodology, with including fibrous structures, can lead to elegant modeling of complex cytoskeleton network inside cell models.

Regarding modeling tumor growth process, we have considered an early stage growth of a 2D circular shape tumor with different volumetric fractions of cancerous cells inside. According to the presented results, we have showed that the applied methodology is accurate, with a potential to investigate additional conditions; effects on the tumor growth of stiffness of different compartments, and the slipping between supporting domain and other compartments. This methodology can also be extended to 3D problems, which would lead to more realistic models of volumetric deformations with geometry obtained from CT scans or uMRIs. The introduced concept is in the developing stage offering a basis that can further be modified and improved.

ACKNOWLEDGMENTS:

The authors acknowledge support from Ministry of Education, Science and Technological Development of the Republic of Serbia and City of Kragujevac, Serbia.

CONFLICT OF INTEREST:

The authors declare that they have no conflict of interest.

FUNDING:

This research is supported by the European Union's Horizon 2020 research and innovation programme under grant agreement No 952603 (http://sgabu.eu/). This article reflects only the author's view. The Commission is not responsible for any use that may be made of the information it contains. Research is also supported by the Ministry of Education, Science and Technological Development of the Republic of Serbia, contract number [451-03-68/2022-14/ 200378 (Institute of Information Technologies, University of Kragujevac)].

REFERENCES:

[1] Kojic M, Smeared concept as a general methodology in finite element modeling of physical fields and mechanical problems in composite media. J. Serb. Soc. Comput. Mech. 2018; 12(2); 16.

[2] Kojic M, Milosevic M, Ziemys A, Computational Models in Biomedical Engineering – Finite Element Models Based on Smeared Physical Fields - Theory, Solutions and Software, Elsevier 2022 (to be published).

[3] Keeley ML, Molecular assembly and mechanical properties of the extracellular matrix: A fibrous protein perspective. Biochimica et Biophysica Acta (BBA) - Molecular Basis of Disease 2013; 1832(7); 866-875.

[4] Bell E, Ivarsson B, Merrill C, Production of a tissue-like structure by contraction of collagen lattices by human fibroblasts of different proliferative potential in vitro. Proc. Natl. Acad. Sci 1979; 76; 1274-1278.

[5] Grinnell F, Fibroblasts, myofibroblasts, and wound contraction. J. Cell Biol. 1994; 124; 401-404.

[6] Goeckeler ZM, Myosin light chain kinase-regulated endothelial cell contraction: the relationship between isometric tension, actin polymerization, and myosin phosphorylation. J. Cell Biol. 1995; 130; 613-627.

[7] Kolodney MS, Correlation of myosin light chain phosphorylation with isometric contraction of fibroblasts. J. Biol. Chem. 1993; 268; 23850-23855.

[8] Sowers GF, Introductory Soil Mechanics and Foundations: Geotechnical Engineering, Prentice-Hall 1979.

[9] Kojić M, Filipovic N, Stojanovic B, Kojic N, Computer Modeling in Bioengineering: Theoretical background, examples and software, John Wiley & Sons 2008.

[10] De Borst R, Non-orthogonal cracks in a smeared finite element model. Engineering Computations 1985; 2(1); 35-46.

[11] Kojic M, Milosevic M, Simic V, Koay EJ, Fleming JB, Nizzero S, et al. A composite smeared finite element for mass transport in capillary systems and biological tissue. Comp. Meth. Appl. Mech. Engrg. 2017; 324; 413–437.

[12] Kojic M, Milosevic M, Simic V, Koay EJ, Kojic N, Ziemys A, et al. Extension of the Composite Smeared Finite Element (CSFE) to Include Lymphatic System in Modeling Mass Transport in Capillary Systems and Biological Tissue. J. Serb. Soc. Comp. Mech. 2017; 11(2); 108-120.

[13] Milosevic M, Simic V, Milicevic B, Koay EJ, Ferrari M, Ziemys A, et al. Correction function for accuracy improvement of the Composite Smeared Finite Element for diffusive transport in biological tissue systems. Comp. Meth. Appl. Mech. Engrg. 2018; 338; 97-116.

[14] M. Kojic, N. Filipovic, M. Zivkovic, R. Slavkovic, N. Grujovic, and M. Milosevic, “PAK Finite Element Program.” University of Kragujevac, Serbia and R&D Center for Bioengineering, Kragujevac, Serbia, 2018.

[15] Zanetti-Dallenbach R, Plodinec M, Oertle P, Redling K, Obermann EC, Lim YHR, et al. Length Scale Matters: Real-Time Elastography versus Nanomechanical Profiling by Atomic Microscopy for the Diagnosis of Breast Lesions. BioMed Research International Hindawi 2018; 1-13.

[16] Santagiuliana R, Milosevic M, Milicevic B, Sciume G, Simic V, Ziemys A, et al. Coupling tumor growth and bio distribution models, Biomedical Microdevices 2019; 21 (2); doi: 10.1007/s10544-019-0368-y

[17] Sciumè G, Shelton S, Gray W, Miller C, Hussain F, Ferrari M, et al. A multiphase model for three-dimensional tumor growth, New Journal of Physics 2013; 15(1)

[18] Wang Z, Butner J. D, Kerketta R, Cristini V, Deisboeck T. S, Simulating cancer growth with multiscale agent-based modeling. Seminars Canc. Biol. 2015; 30, 70–78

[19] Kim Y, Othmer H. G. Hybrid models of cell and tissue dynamics in tumor growth. Math. Biosc. Engrg. 2015; 12 (6), 1141-1156.

FIGURE CAPTIONS:

Figure 1. a) 2D schematic representation of a "detailed" model of a composite medium (with denoted subdomains; extracellular space with embedded cells, organelles of cells and fibrous structure). b) Smeared representation of detailed a) model with noted velocities and stresses (in normal and tangent directions) at the common boundaries. c) Contact between two immersed domains (here noted as Cells 7 and 8) with contact boundary and velocities displayed d) Contact between supporting domain and immersed domain (here noted as 'b' and Cell 78) with contact boundary and velocities displayed.

Figure 2. Composite smeared finite element for mechanics, CSFEM, (3D representation). The element volume dV is composed of the supporting medium (volume V^b) and subdomains (compartments with volumes V^1 to V^K). The nodal degrees of freedom include velocities of the supporting medium and immersed domains. Contact elements are used to couple velocities at the domain contact boundaries.

Figure 3. a) Detailed model of pancreatic tumor tissue with 80 cells. b) Smeared model with tissue and cells domain.

Figure 4. (a) Detailed model with cells compared to the smeared model (b). Displacement field at time steps t=2.5s (random time step in loading direction), 5.0s (maximum displacement in the x-direction), and t= 7.5s- (random time step in reverse loading direction). Young's moduli in the surrounding domain and cells are equal.

Figure 5. a) Example of representative AFM map (20 × 20 x 5 μm) with stiffness field displayed [15]. b) Test example 100x50 constrained and loaded in x-direction (Two last nodes on the right border, in the right corner).

Figure 6. Displacement field in the x-direction for supporting medium, (cases with and without slipping), and compartment displacement. The initial configuration is given with a black dashed line.

Figure 7. Displacement vs. Force diagram for Supporting medium, for cases with and without slipping, and compartment. The resistance coefficient between the compartment and supporting domain, in case of slipping, is $\eta_1 = 10$.

Figure 8. a) Model of circular tumor domain and surrounding tissue, 1/4 of the entire space due to symmetry. Sliding is allowed along the boundary lines (x and y-axis) b) CSFE mesh of model generated in our in-house software CAD (number of FE nodes is 56 085, number of 2D elements is 32 254)

Figure 9. Displacement field for 2 different time steps and 3 different volumetric fractions of cells inside area divided by internal radius- R_{tum} = 3mm (area specified by black dashed line). The black continuous line indicates how much area, in which we have specified different volumetric fraction cases (r_V =0.3-0.5-0.7), had grown during the simulation process; the red chain line indicates the initial tissue boundary).

Figure 10. Diagram of tumor radius increase over time for 3 volumetric fraction values of cancerous cells (initial radius of tumor is R_{tum} = 3 mm).

Figure 11. Displacement field for two time steps and three volumetric fractions of cells inside the area bounded by the internal radius- R_{tum} = 7mm (area specified by black dashed line). The black continuous line indicates how much area, in which we have specified volumetric fraction cases (r_V =0.3-0.5-0.7), had grown during the the growth process; the red chain line indicates the initial tissue boundary).

Figure 12. Diagram of tumor radius increase over time for three volumetric fraction values of cancerous cells (initial radius of tumor is R_{tum} = 7 mm)

FIGURES:

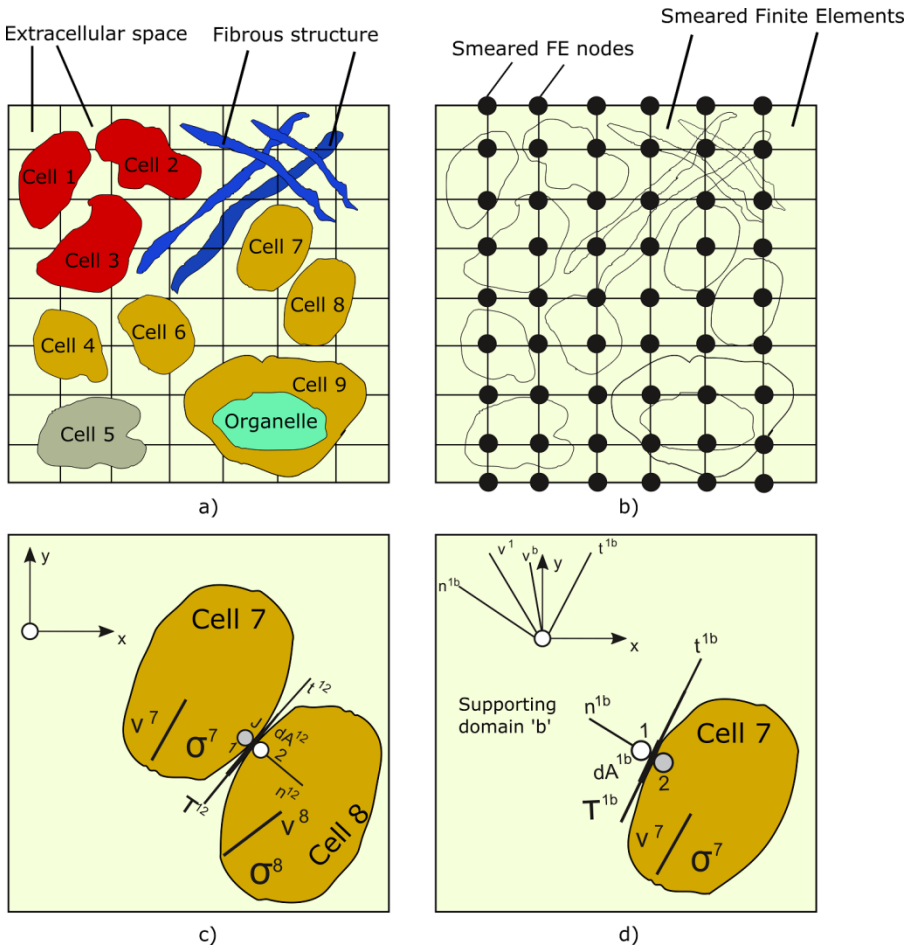

Figure 1.

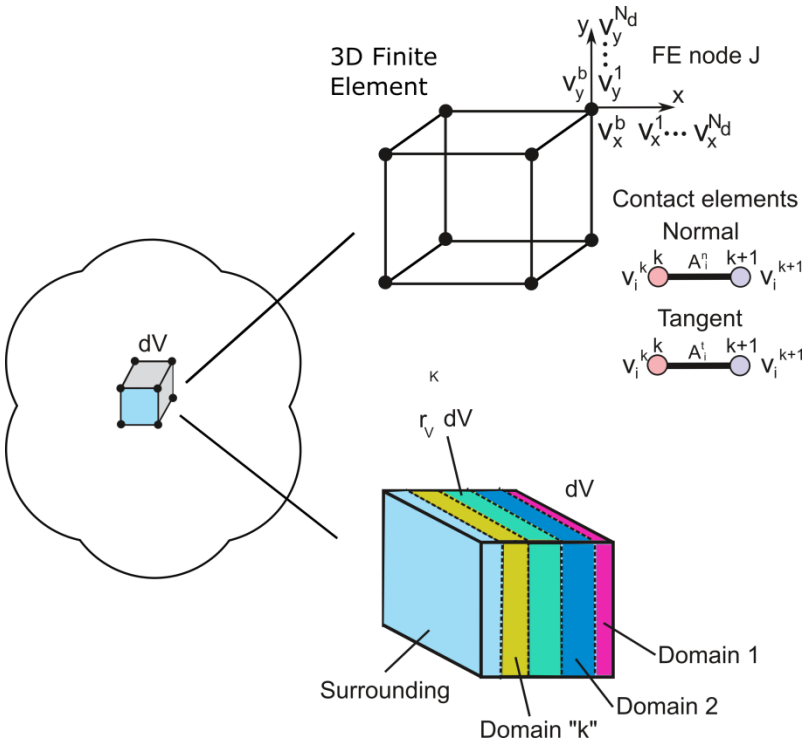
3D Finite
Element
FE node J
Contact elements
Normal
Tangent
dV
dV
Surrounding
Domain 1
Domain 2
Domain "k"

Figure 2.

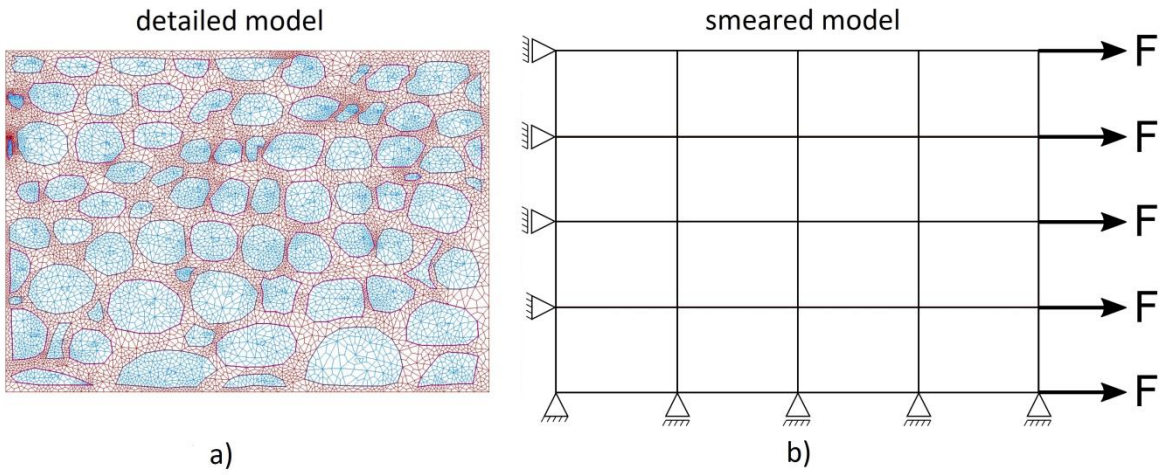

Figure 3.

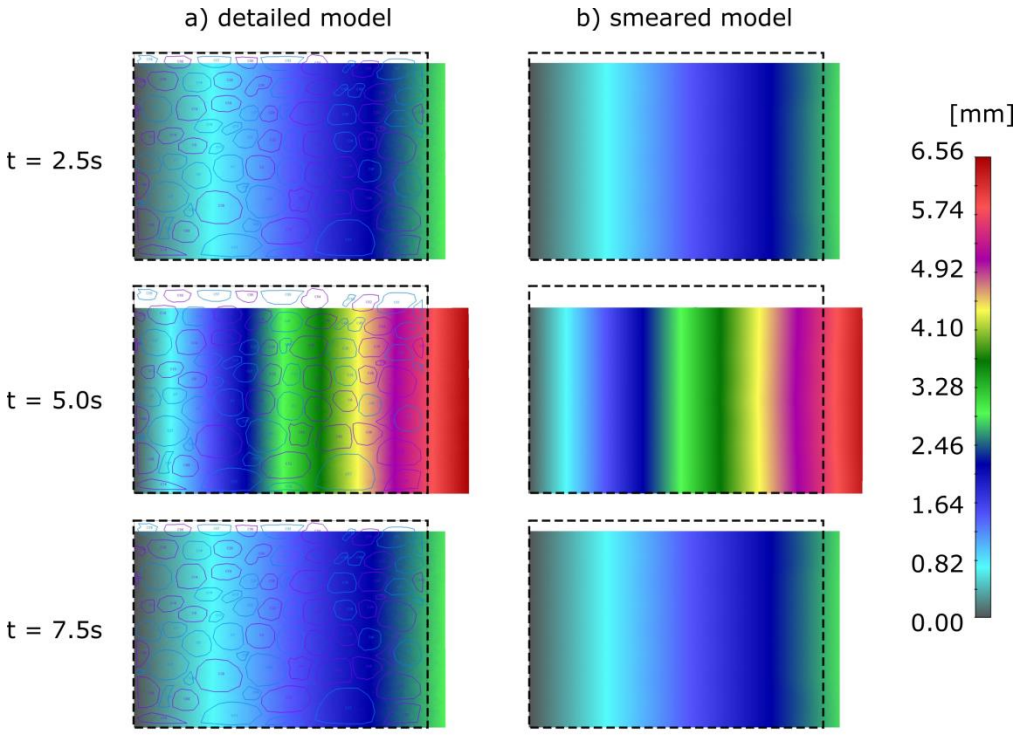
a) detailed model
b) smeared model
t = 2.5s
t = 5.0s
t = 7.5s
[mm]
6.56
5.74
4.92
4.10
3.28
2.46
1.64
0.82
0.00

Figure 4.

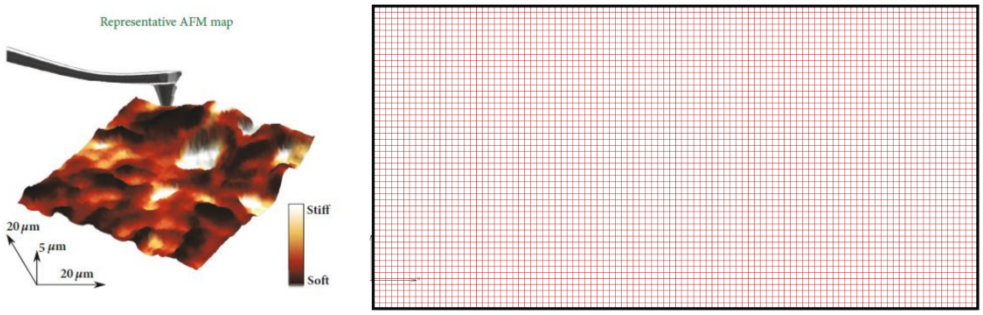

Figure 5.

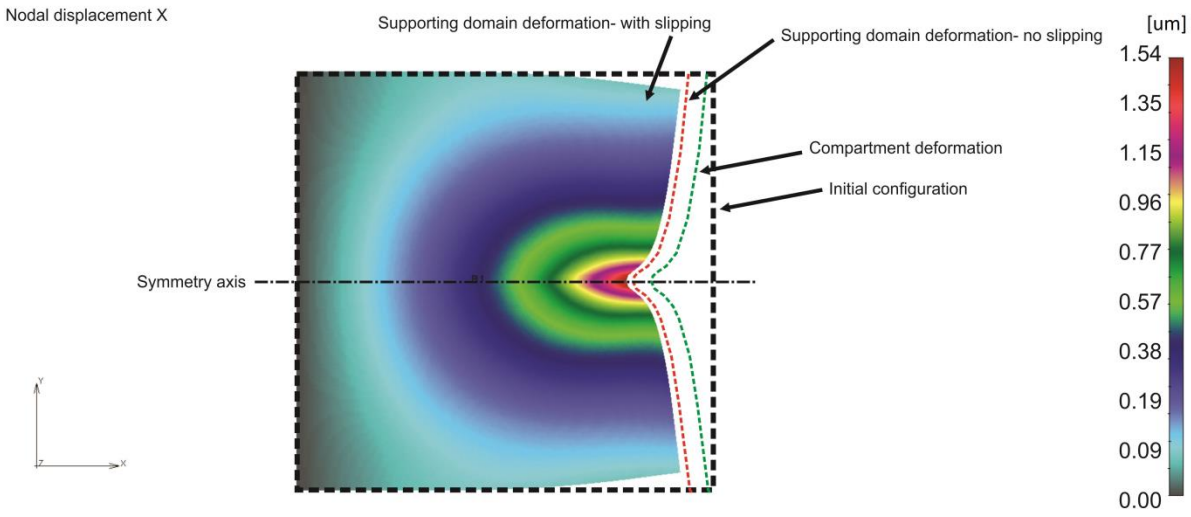
Nodal displacement X
Supporting domain deformation- with slipping
Supporting domain deformation- no slipping
Compartment deformation
Initial configuration
Symmetry axis
[um]
1.54
1.35
1.15
0.96
0.77
0.57
0.38
0.19
0.09
0.00

Figure 6.

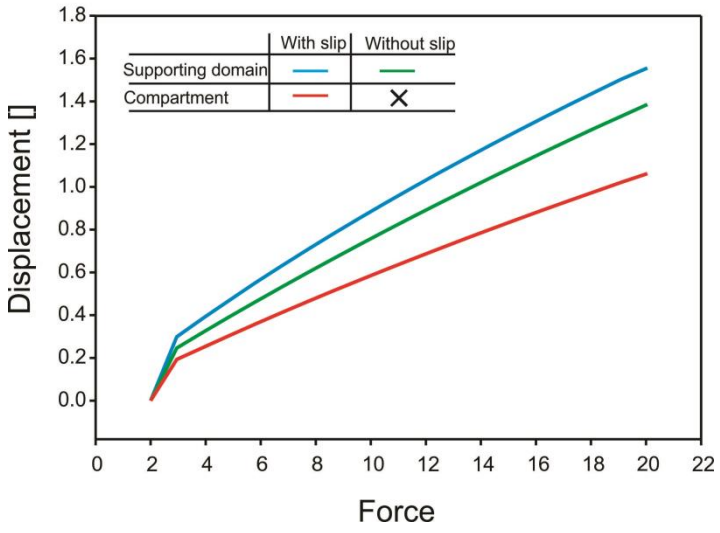
With slip
Without slip
Supporting domain
Compartment
Displacement []
Force
1.8
1.6
1.4
1.2
1.0
0.8
0.6
0.4
0.2
0.0
0
2
4
6
8
10
12
14
16
18
20
22

Figure 7.

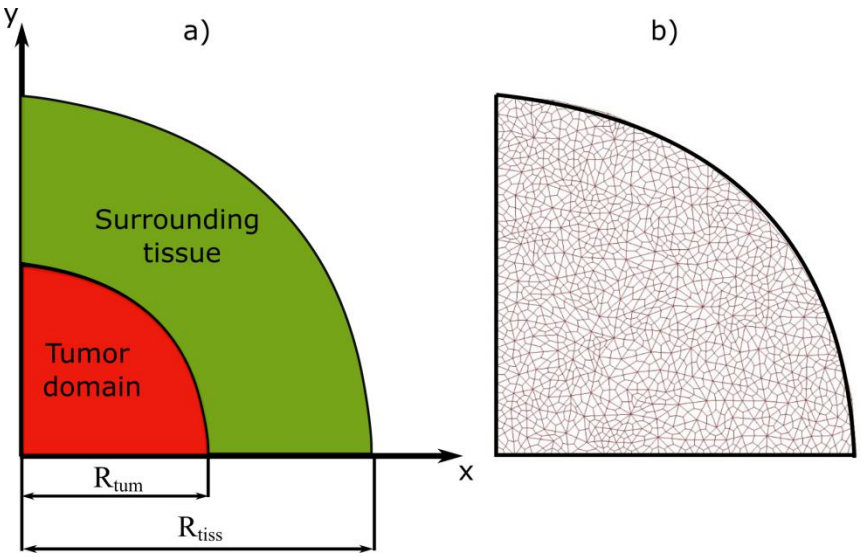

Figure 8.

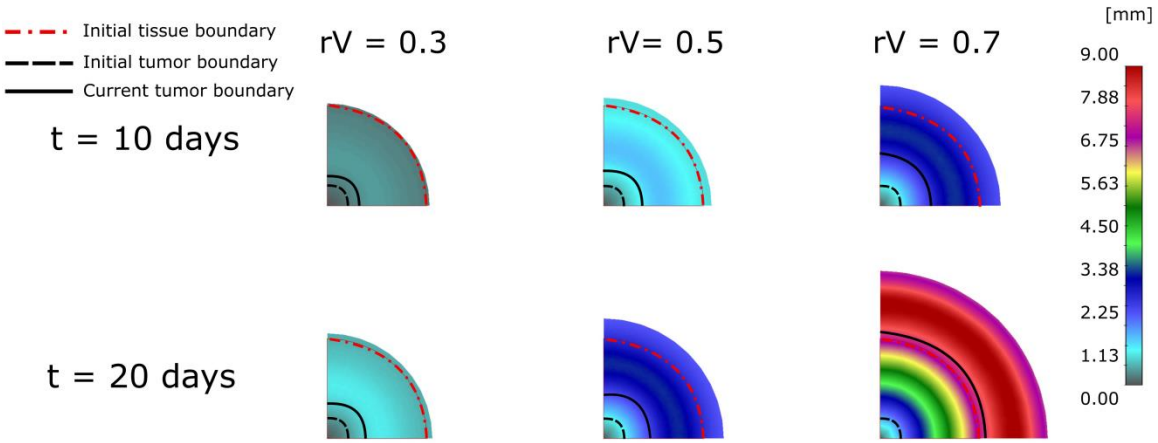
Initial tissue boundary
Initial tumor boundary
Current tumor boundary
rV = 0.3
rV= 0.5
rV = 0.7
[mm]
9.00
7.88
6.75
5.63
4.50
3.38
2.25
1.13
0.00
t = 10 days
t = 20 days

Figure 9.

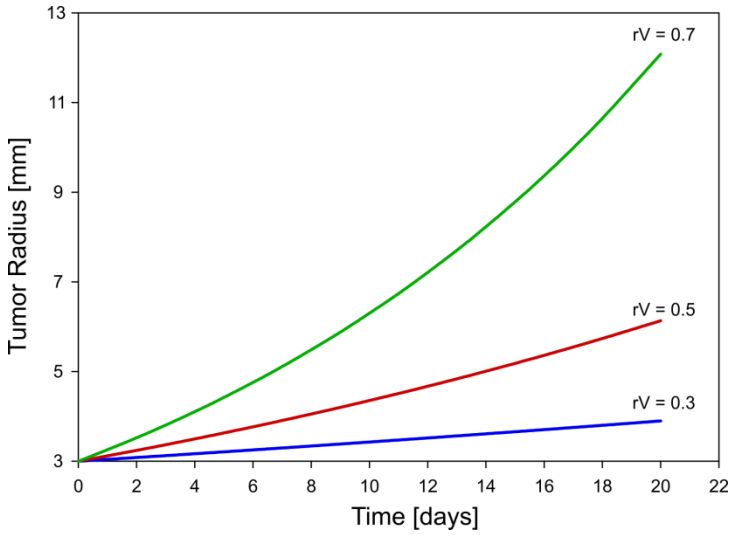
Tumor Radius [mm]
Time [days]
rV = 0.7
rV = 0.5
rV = 0.3
13
11
9
7
5
3
0
2
4
6
8
10
12
14
16
18
20
22

Figure 10

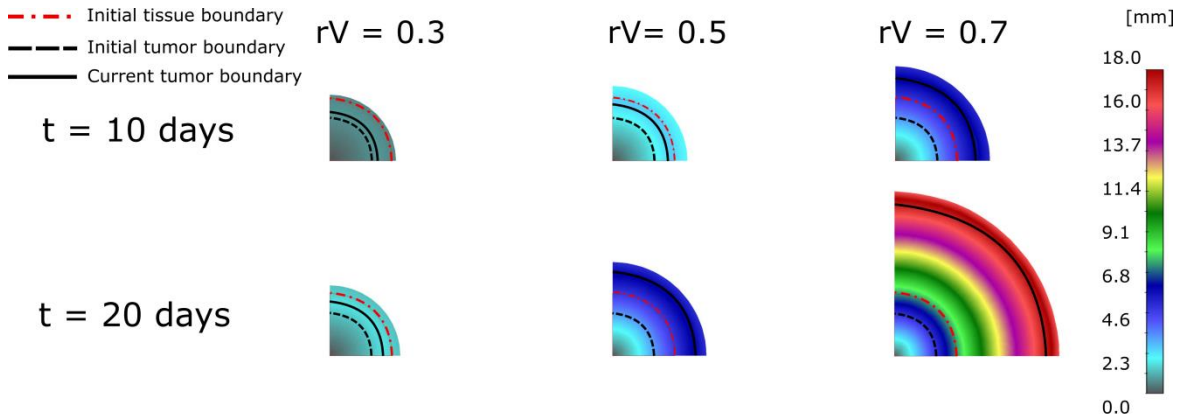
Initial tissue boundary
Initial tumor boundary
Current tumor boundary
rV = 0.3
rV= 0.5
rV = 0.7
[mm]
18.0
16.0
13.7
11.4
9.1
6.8
4.6
2.3
0.0
t = 10 days
t = 20 days

Figure 11

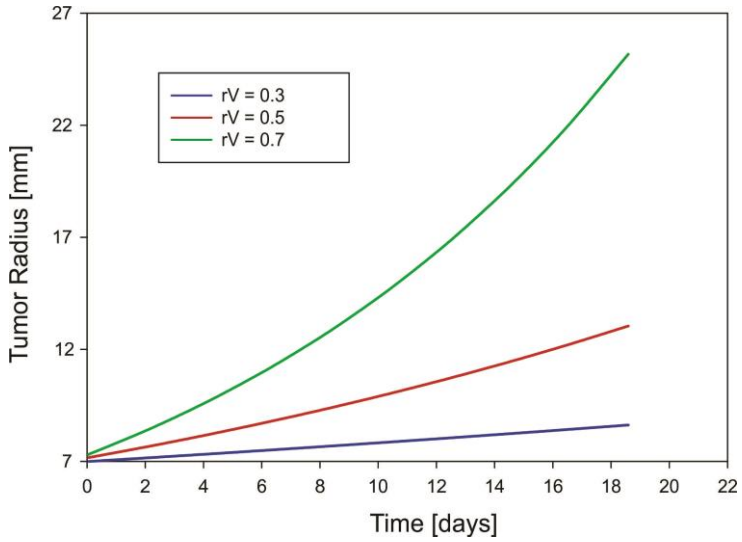
rV = 0.3
rV = 0.5
rV = 0.7
Tumor Radius [mm]
27
22
17
12
7
0
2
4
6
8
10
12
14
16
18
20
22
Time [days]

Figure 12